

# Loss of coupling between calcium influx, energy consumption and insulin secretion associated with development of hyperglycaemia in the UCD-T2DM rat model of type 2 diabetes

A. M. Rountree · B. J. Reed · B. P. Cummings ·  
S.-R. Jung · K. L. Stanhope · J. L. Graham ·  
S. C. Griffen · R. L. Hull · P. J. Havel · I. R. Sweet

Received: 8 October 2012 / Accepted: 3 December 2012 / Published online: 13 February 2013  
© Springer-Verlag Berlin Heidelberg 2013

## Abstract

**Aims/hypothesis** Previous studies on isolated islets have demonstrated tight coupling between calcium ( $\text{Ca}^{2+}$ ) influx and oxygen consumption rate (OCR) that is correlated with insulin secretion rate (ISR). To explain these observations, we have proposed a mechanism whereby the activation of a highly energetic process ( $\text{Ca}^{2+}$ /metabolic coupling process [CMCP]) by  $\text{Ca}^{2+}$  mediates the stimulation of ISR. The aim of the study was to test whether impairment of the CMCP could play a role in the development of type 2 diabetes.

**Methods** Glucose- and  $\text{Ca}^{2+}$ -mediated changes in OCR and ISR in isolated islets were compared with the time course of changes of plasma insulin concentrations observed during the progression to hyperglycaemia in a rat model of type-2 diabetes (the University of California at Davis type 2 diabetes mellitus [UCD-T2DM] rat). Islets were isolated from UCD-T2DM rats before, 1 week, and 3 weeks after the onset of hyperglycaemia.

**Results** Glucose stimulation of cytosolic  $\text{Ca}^{2+}$  and OCR was similar for islets harvested before and 1 week after the onset of hyperglycaemia. In contrast, a loss of decrement in islet OCR and ISR in response to  $\text{Ca}^{2+}$  channel blockade coincided with decreased fasting plasma insulin concentrations observed in rats 3 weeks after the onset of hyperglycaemia. **Conclusions/interpretation** These results suggest that phenotypic impairment of diabetic islets in the UCD-T2DM rat is downstream of  $\text{Ca}^{2+}$  influx and involves unregulated stimulation of the CMCP. The continuously elevated levels of CMCP induced by chronic hyperglycaemia in these islets may mediate the loss of islet function.

**Keywords** Calcium · Hyperglycaemia · Insulin secretion · Islets · Oxygen consumption

## Abbreviations

CMCP	$\text{Ca}^{2+}$ /metabolic coupling process
FCCP	Carbonyl cyanide- <i>p</i> -trifluoromethoxyphenylhydrazone
ER	Endoplasmic reticulum
ISR	Insulin secretion rate
OCR	Oxygen consumption rate
UCD-T2DM	University of California at Davis type 2 diabetes mellitus

A. M. Rountree · B. J. Reed · S.-R. Jung · I. R. Sweet (✉)  
Diabetes and Obesity Center of Excellence, University of  
Washington, 850 Republican Street,  
Seattle, WA 98109-8055, USA  
e-mail: isweet@u.washington.edu

B. P. Cummings · K. L. Stanhope · J. L. Graham · P. J. Havel  
Department of Molecular Biosciences, School of Veterinary  
Medicine and Department of Nutrition, University of California,  
Davis, CA, USA

S. C. Griffen  
Bristol-Myers Squibb, Princeton, NJ, USA

R. L. Hull  
Department of Medicine, VA Puget Sound Health Care System and  
University of Washington, Seattle, WA, USA

## Introduction

An essential step triggering insulin secretion by pancreatic beta cells is closure of  $\text{K}_{\text{ATP}}$  channels leading to the opening of voltage-dependent  $\text{Ca}^{2+}$  channels [1]. Increased

metabolic rate generates another essential signal, without which increased  $\text{Ca}^{2+}$  influx does not stimulate ISR [2, 3]. A number of factors generated by increased metabolism have been proposed including NADPH [4], fatty-acid signalling [5], ATP/ADP ratio [6], cytochrome *c* [7], mitochondrial GTP [8], reactive oxygen species [9] and factors associated with pyruvate carboxylase and anaplerosis [10–12]. How beta cells integrate both  $\text{Ca}^{2+}$  and metabolic factors is not understood, but we have hypothesised the existence of a cascade of steps that are dually regulated by these two factors and govern the triggering of insulin secretion [13]. We have named this process, linking the  $\text{Ca}^{2+}$  signal with insulin secretion, the ‘ $\text{Ca}^{2+}$ /metabolic coupling process (CMCP)’ and have sought to characterise its defining features by quantifying metabolic and electrophysiological variables of isolated islets [13, 14]. The major identifier of the CMCP is its use of approximately 35% of glucose-stimulated energy production, which cannot be accounted for by the energy used in exocytosis of secretory granules [15]. The CMCP can be quantified by the decrement of glucose-stimulated oxygen consumption rate (OCR) in response to blocking the influx of  $\text{Ca}^{2+}$ , a variable reflecting the work associated with  $\text{Ca}^{2+}$ -activated processes [15]. The link between OCR and ATP usage is supported by studies demonstrating that the majority of ATP is generated by mitochondrial respiration [16]. Importantly, the OCR linked to the CMCP is highly correlated with substrate-stimulated insulin secretion rate (ISR) [15], and its activation is essential for sustained insulin secretion to occur [13]. Like ISR, it is under dual control by both  $\text{Ca}^{2+}$  entering the cell via L-type  $\text{Ca}^{2+}$  channels [14] and metabolic rate [13]. Finally the process is upstream of potentiation of glucose-stimulated ISR by protein kinases whereby ISR is increased without significantly altering OCR [14, 15]. These observations lead us to hypothesise that the combination of  $\text{Ca}^{2+}$  influx and metabolic rate leads to the activation of a highly energetic process (CMCP) that couples  $\text{Ca}^{2+}$  to its effect on ISR [13].

To further establish the validity of this hypothesis, we tested whether impairment of the CMCP could play a role in the progression of type 2 diabetes. The approach taken involved measurements on islets isolated from diabetic rats at different stages in the development of hyperglycaemia and decreased insulin secretion. The diabetic rat model used (University of California at Davis type 2 diabetes mellitus [UCD-T2DM]) was generated by crossing obese insulin-resistant Sprague–Dawley rats with ZDF-lean rats, which have a defect in beta cell function [17]. The progression of glycaemic control in the model was characterised by euglycaemia in the young rats, followed by steadily increasing circulating glucose levels accompanied by increased ISR. After onset of hyperglycaemia, by 3 weeks ISR declined and by 3 months a large fraction of the beta cells were destroyed. Previous studies carried out on islets from these rats

indicated that loss of secretory function did not correlate with loss of islet volume or number [17]. Therefore, we concluded that impaired islet secretory function was likely to underlie the decreased plasma insulin concentrations observed concomitant with increasing glucose levels, and that the UCD-T2DM rat was an appropriate animal model with which to investigate the longitudinal role of the CMCP in islet function.

The aim of the study, therefore, was to investigate the intracellular mechanisms responsible for the impaired secretory function that develops between 1 and 3 weeks after onset of hyperglycaemia. Isolated islets underwent analysis of multiple variables reflecting sequential components in the stimulus–secretion coupling pathway. Thus, glucose stimulation of metabolism was assessed by increases in OCR, opening of voltage-dependent  $\text{Ca}^{2+}$  channels was assessed by cytosolic  $\text{Ca}^{2+}$  and activation of the CMCP was assessed by the decrement in OCR in response to blocking  $\text{Ca}^{2+}$  influx. These variables were compared longitudinally with plasma insulin concentrations measured *in vivo* to determine which step(s) were associated with the decline of islet secretory function. Based on standard analysis of islet metabolic and  $\text{Ca}^{2+}$  response, the islets appeared functionally intact. However, our results showed that dysregulation of the CMCP occurring downstream of  $\text{Ca}^{2+}$  entry is associated with markedly reduced ISR and plasma insulin concentrations during the transition to hyperglycaemia/overt diabetes.

## Methods

**Chemicals** KRB supplemented with 20 mmol/l HEPES/NaHEPES (Roche, Indianapolis, IN, USA) and 0.1% bovine serum albumin (Serological Corporation, Norcross, GA, USA) was used for perfusion experiments and was made as previously described [15].

**Animals** Male UCD-T2DM rats were housed in the animal facility in the Department of Nutrition at the University of California, Davis and maintained on a 14:10-h light–dark cycle. Rats characterised as hyperglycaemic or diabetic (blood glucose >11.1 mmol/l for 2 consecutive days [17]), were studied either 1 week or 3 weeks after onset. Blood glucose was determined on 5  $\mu\text{l}$  of whole blood using a OneTouch Glucometer (Lifescan, Milpitas, CA, USA). Male Sprague–Dawley rats (used as controls) were purchased from Harlan (Livermore, CA, USA). The experimental protocols were approved by the Institutional Animal Care and Use Committees of the Universities of Washington and California, Davis.

**Rat islet isolation and culture** Islets were harvested by collagenase digestion of the pancreas and purified as

previously described [18, 19]. Rats were anaesthetised by intraperitoneal injection of sodium pentobarbital (35 mg/230 g rat). Before the experiments islets were cultured for 18 h at 37°C in RPMI Medium 1640 containing 10% fetal bovine serum (Invitrogen, Carlsbad, CA, USA).

**Measurement of OCR, cytochrome *c* reduction and ISR** A perfusion system was used that concomitantly measured OCR and cytochrome *c* reduction while collecting outflow fractions for subsequent determination of ISR [18, 20, 21]. Islets (125–175) were loaded into in each of two perfusion chambers. OCR was calculated as flow rate (30–40  $\mu\text{l}/\text{min}$ ) multiplied by the difference between inflow and outflow oxygen tension measured by detecting the phosphorescence lifetime (MFPF-100; Tau Theta, Boulder, CO, USA) of an oxygen-sensitive dye painted on the inside of the perfusion chamber [15]. Absorption by cytochrome *c* was measured by light transmitted at 550 nm through the bed of islets/Cytodex beads [18]. Insulin was measured by ELISA (Merckodia, Uppsala, Sweden) or RIA (Millipore Corporation, Billerica, MA, USA).

**Automated histological determination of beta cell area** Formalin-fixed, paraffin-embedded pancreas sections (5  $\mu\text{m}$ ) were stained with anti-insulin antibody (1:2,000; Sigma-Aldrich, St Louis, MO, USA) followed by biotinylated goat anti-mouse IgG (1:500; Jackson ImmunoResearch, West Grove, PA, USA), Vector ‘Elite’ ABC-HP (Burlingame, CA, USA), 3,3'-diaminobenzidine substrate and haematoxylin counterstain and then mounted on coverslips. Whole slide images were generated using a Nanozoomer Digital Pathology slide scanner (Olympus America, Center Valley, PA, USA). The insulin-positive area was computed based on pixel colour and density for each section using Visiopharm software (Hoersholm, Denmark) and verified by manual examination of segmented images. Total (100%) section area ( $149 \pm 8 \text{ mm}^2$ , mean  $\pm$  SEM) was assessed, and total pancreas area was determined as the sum of insulin-negative and insulin-positive pancreas areas.

**Insulin content** Insulin content per islet was determined in wells of 24-well plates (in triplicate) containing five islets in 0.2 ml of culture media, after adding 1 ml of a hydrochloric acid/95% ethanol mixture (2% vol./vol.) and incubating for 60 min. After centrifugation at 800g for 5 min, the supernatant fraction was transferred to fresh tubes, and insulin was measured by ELISA (Merckodia). For some experiments, islet insulin content was measured immediately following their isolation, and no differences were seen relative to islets cultured overnight (data not shown).

**Imaging and quantification of cytosolic  $\text{Ca}^{2+}$**  Cytosolic  $\text{Ca}^{2+}$  was measured by fluorescence imaging after islets were

incubated in 2  $\mu\text{mol}/\text{l}$  Fura-2 AM (Invitrogen) and 0.02% pluronic acid for 40 min at 37°C and perfused in KRB (containing 5 mmol/l  $\text{NaHCO}_3$ ) as previously described [22]. Results are displayed as the ratio of the fluorescent intensity during excitation at either 340 or 380 nm (F340/F380).

**Plasma glucose and insulin measurements** Blood samples were collected after an overnight (12 h) fast from the tails of male UCD-T2DM rats ( $n=7$  per group). Non-fasting blood glucose concentrations were measured before fasting (at 14:00–16:00 hours) using a glucometer. Plasma was assayed for glucose and insulin concentrations using an enzymatic colorimetric assay (Thermo DMA, Louisville, CO, USA) and ELISA (Millipore, St Charles, MO, USA), respectively.

**Perfusion protocols and data analysis** The basic protocol for the OCR, ISR and  $\text{Ca}^{2+}$  perfusion experiments entailed a 90-min baseline period at 3 mmol/l glucose followed by stimulation with 20 mmol/l glucose for 60 min and subsequent inhibition of  $\text{Ca}^{2+}$  influx with 5  $\mu\text{mol}/\text{l}$  nimodipine for 60 min. OCR data are displayed as the change relative to the baseline calculated as the average of values obtained between  $-10$  and  $0$  min. To assess mitochondrial uncoupling in islets, the protocol entailed the inhibition of the  $\text{F}_0\text{F}_1\text{ATPase}$  with oligomycin to remove the coupled portion of OCR [23, 24], followed by the addition of a mitochondrial uncoupler (FCCP). Steady-state values were calculated as the average of the final 10 min of each experimental condition. Statistical significance ( $p$  values) was generated from the calculation of ANOVA with a post hoc Bonferonni test using Kaleidagraph (Synergy Software, Reading, PA, USA), except for the immunohistochemical data upon which a Student's  $t$  test using Microsoft Excel (Redmond, WA, USA) was performed.

## Results

**Animal characteristics** Islets from three groups of UCD-T2DM rats were compared: euglycaemic, and 1 or 3 weeks after the diagnosis of hyperglycaemia (fed blood glucose concentrations  $>11.1$  mmol/l for two consecutive measurements). Age, weight and blood glucose levels were recorded for all rats just before islet harvest (Table 1). The ages and weights of the three groups of UCD-T2DM rats were similar. Blood glucose concentrations were approximately two-fold higher in the rats 1 week after onset of hyperglycaemia relative to euglycaemic rats ( $p<0.001$ ) and further increased to approximately threefold higher in the rats 3 weeks post onset ( $p<0.001$ ). Control data were obtained from islets isolated from Sprague–Dawley rats, which were slightly younger and lighter than the UCD-T2DM rats. A second

**Table 1** Characteristics of UCD-T2DM and control rats

Characteristic	Control	UCD-T2DM		
		Pre-onset	1 week post-onset	3 weeks post-onset
Number of rats	5	8	8	8
Age (weeks)	8.0±0.1	10.9±0.2	10.7±0.5	11.7±0.1
Weight (g)	402±4	440±13	440±34	444±12
Blood glucose (mmol/l)	7.6±0.5	6.8±0.5	12.2±2.1***	18.9±2.0***

Values are average±SEM

Age, weight and blood glucose were recorded immediately before harvesting the islets. UCD-T2DM rats used in the study were either normoglycaemic or had become hyperglycaemic 1 or 3 weeks before harvesting their islets for assessment. Sprague–Dawley rats were used as a source of control islets

\*\*\* $p < 0.001$  generated from an ANOVA on the UCD-T2DM rats with a post hoc Bonferonni test carried out using Kaleidagraph (Synergy Software). The two values with asterisks were found to be statistically different from the pre-onset values

cohort of male UCD-T2DM rats were used to characterise circulating glucose and insulin concentrations at times corresponding to the times that the islet measurements were made. Non-fasting blood glucose was significantly elevated in UCD-T2DM rats 1 and 3 weeks after onset of hyperglycaemia (Fig. 1). Insulin was elevated 1 week following onset but decreased by 3 weeks despite the continued hyperglycaemia.

**Assessment of the CMCP in control islets** To determine whether disruption of the CMCP was associated with the loss of regulated insulin secretion occurring 1–3 weeks following onset of hyperglycaemia, we first measured variables reflecting the operation of the CMCP in islets harvested from control Sprague–Dawley rats. As expected, all three measurements increased robustly in response to increased glucose concentrations (Fig. 2). The subsequent blockade of  $\text{Ca}^{2+}$  influx by L-type  $\text{Ca}^{2+}$  channels (with 5  $\mu\text{mol/l}$  nimodipine) decreased steady-state OCR by  $0.16 \pm 0.03$  (about

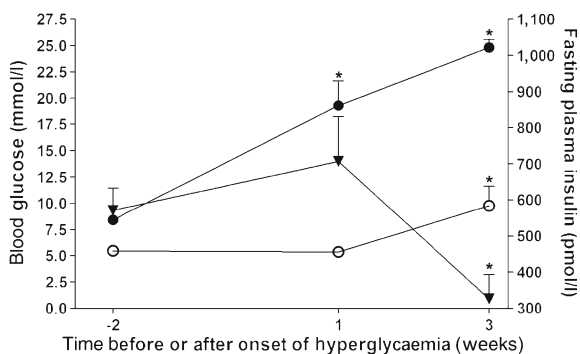


**Fig. 1** Circulating glucose and insulin concentrations at 2 weeks before, and 1 and 3 weeks after, the onset of diabetes in the UCD-T2DM rat. Non-fasting blood glucose (black circle), fasting plasma glucose (white circle) and fasting plasma insulin concentrations (triangle) were plotted as a function of time before and after onset of hyperglycaemia. Values are mean±SEM. \* $p < 0.05$  by Student's *t* test compared with value at 2 weeks before onset

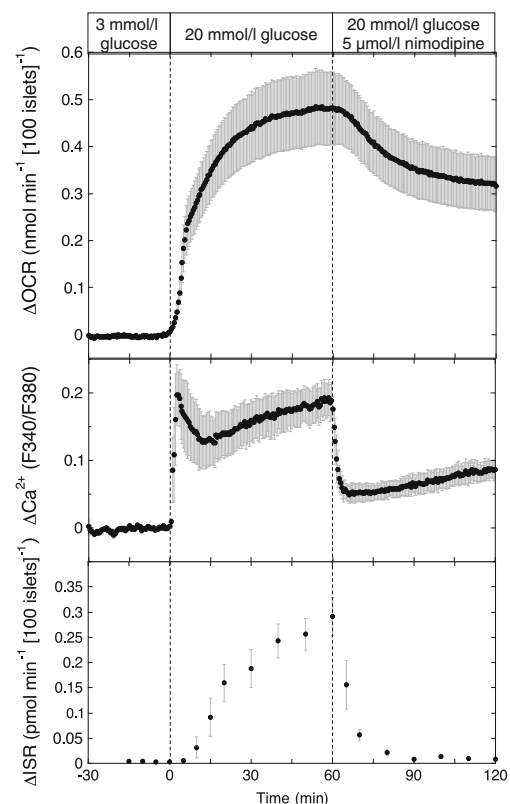


**Fig. 2** Effect of blocking  $\text{Ca}^{2+}$ -influx through L-type  $\text{Ca}^{2+}$  channels on OCR,  $\text{Ca}^{2+}$  and ISR by islets isolated from normoglycaemic Sprague–Dawley rats that were stimulated with 20 mmol/l glucose. Islets were perfused in the presence of 3 mmol/l glucose for 90 min then 20 mmol/l for 60 min, followed by the addition of 5  $\mu\text{mol/l}$  nimodipine. OCR and ISR were measured concomitantly using the flow culture system ( $n=5$ ). Detection of cytosolic  $\text{Ca}^{2+}$  by fluorescence imaging was measured in separate experiments ( $n=3$ ). Data are means±SEM and are displayed as the change in signal relative to the steady-state value obtained at 3 mmol/l glucose. Steady-state values of OCR and ISR at 3 mmol/l glucose are listed in Table 2. Statistical analysis was carried out by comparing steady-state values before and after each change in media composition using a paired *t* test

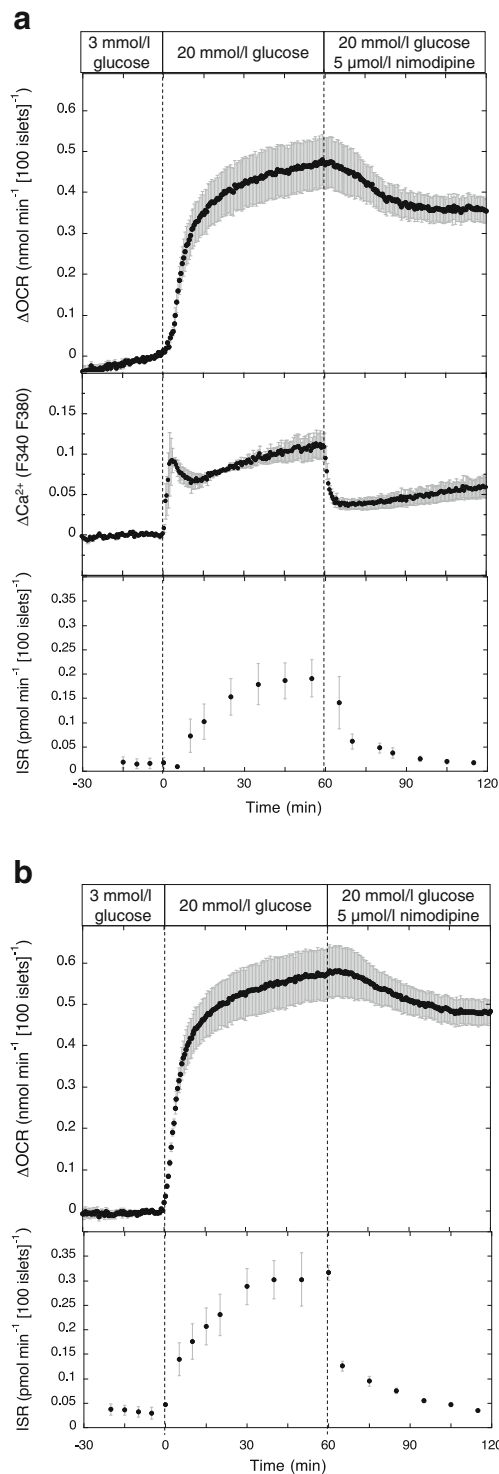


**Fig. 3** Effect of blocking  $\text{Ca}^{2+}$ -influx through L-type  $\text{Ca}^{2+}$  channels on glucose-stimulated islets from UCD-T2DM rats isolated before (**a**), and 1 week (**b**) and 3 weeks (**c**) after, the onset of hyperglycaemia. Islets were perfused using identical protocols to those described in

one third of that stimulated by 20 mmol/l glucose) reflecting the energy used by the CMCP; ISR was completely abolished demonstrating the tight coupling

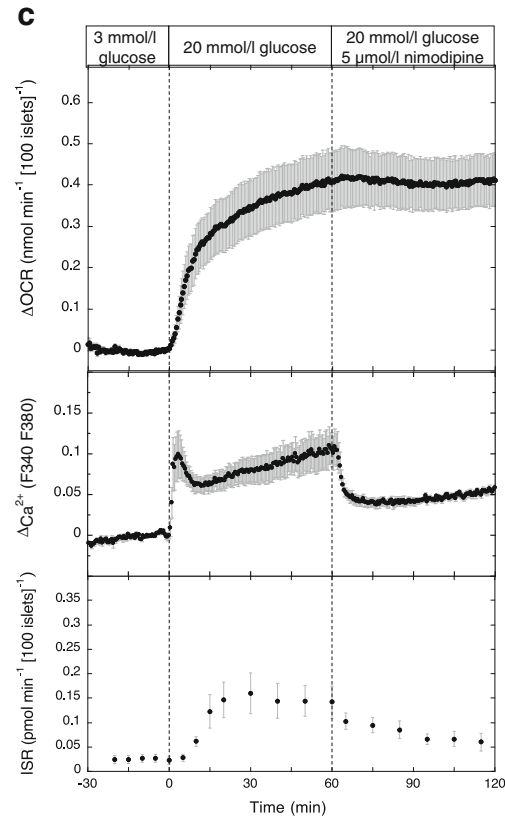


**Fig. 2** except  $\text{Ca}^{2+}$  was not measured for (**b**). Data are displayed and were analysed as described in Fig. 2 legend, except that  $n=8$  for OCR and ISR measurements, and  $n=4$  for  $\text{Ca}^{2+}$  measurements

between  $\text{Ca}^{2+}$  influx, ATP usage and insulin secretion. The  $\text{Ca}^{2+}$  response to glucose was biphasic; due to the slower flow rates required when measuring OCR and

ISR, first phase insulin secretory response to glucose was not observed.

**Loss of  $Ca^{2+}$ -sensitive OCR and ISR in islets occurred in UCD-T2DM rats 3 weeks after onset of hyperglycaemia** To determine which component of stimulus-secretion coupling was correlated with decreased plasma insulin concentrations in UCD-T2DM rats, we repeated the measurements presented in Fig. 2 using isolated islets harvested before, and 1 and 3 weeks after, onset of hyperglycaemia. Islets harvested from UCD-T2DM rats before the onset of hyperglycaemia had normal responses in OCR to glucose, but only ~50% of the  $Ca^{2+}$  and ISR response seen in the islets from control rats (Fig. 3a, Table 2). The OCR responses to nimodipine were qualitatively similar, but the changes were smaller than that for control islets (decrement of OCR as a percentage of the glucose-stimulated increase was 22 vs 34% for the pre-onset and control islets, respectively [Table 2]). Likewise for islets harvested from UCD-T2DM rats 1 week after onset of hyperglycaemia, the two variables reflecting operation of the CMCP, the decrement in OCR and ISR in response to nimodipine (Fig. 3b), were similar to those observed in islets harvested before onset. Notably, glucose-stimulated ISR by islets harvested from rats 1 week after onset of hyperglycaemia was increased by 65% compared with islets harvested from rats before the onset. Islets

harvested 3 weeks after onset of hyperglycaemia exhibited decreased glucose-stimulated ISR, but normal  $Ca^{2+}$  response and only slightly reduced  $\Delta$ OCR in response to 20 mmol/l glucose relative to pre-onset islets (Fig. 3c), indicating that the loss of ISR was not due to the inability of islets to respond to increased metabolism by closure of  $K_{ATP}$  channels. In contrast,  $Ca^{2+}$ -sensitive OCR was nearly completely abolished, and ISR was only partially inhibited by inhibition of  $Ca^{2+}$  influx (Fig. 3c), suggesting that the coupling between  $Ca^{2+}$  influx, energy consumption and ISR was lost.

**Correlation of islet characteristics with longitudinal changes in plasma insulin and glucose levels in UCD-T2DM rats** The steady-state values of measured variables in islets shown in Figs 2 and 3 were tabulated and compared with the longitudinal changes of fasting plasma insulin concentrations in UCD-T2DM rats (Table 2). During the progression from euglycaemia to hyperglycaemia, the responses of ISR measured in vitro mirrored the changes of fasting plasma insulin seen in vivo, while glucose stimulation of OCR and cytosolic  $Ca^{2+}$  in islets remained unchanged. Notably, the disappearance of the  $Ca^{2+}$ -sensitive OCR coincided with the marked decline of plasma insulin concentrations that occurred 3 weeks after the onset of hyperglycaemia.

**Table 2** Steady-state values of OCR, ISR and  $\Delta Ca^{2+}$  calculated from kinetic responses by islets harvested from rats at different stages of glycaemic control

Characteristic	Control	UCD-T2DM		
		Pre-onset	1 week post-onset	3 weeks post-onset
Fasting insulin	ND	433±33	500±42	217±17
OCR <sub>3</sub> mmol/l glc	0.39±0.09	1.4±0.4	1.1±0.2	0.9±0.3
$\Delta$ OCR <sub>20</sub> mmol/l glc	0.48±0.07	0.47±0.06	0.47±0.05	0.41±0.07
% Decrement OCR <sub>nim</sub>	33±2	22±3	16±3	3±3***
ISR <sub>3</sub> mmol/l glc	0.05±0.02	0.1±0.06	0.19±0.03	0.15±0.05
ISR <sub>20</sub> mmol/l glc	1.5±0.2	1.1±0.3	1.9±0.1	0.8±0.2***
% Decrement ISR <sub>nim</sub>	96±1	83±5	88±1	44±7***
$\Delta Ca^{2+}$ 20 mmol/l glc	0.18±0.02	0.12±0.02	ND	0.11±0.01

Data are the average±SEM

Steady-state calculations were made on data from individual experiments (the composites of which are shown in Figs 2, 3, and the number of replicates performed are listed in the figure legends). The changes in OCR and  $Ca^{2+}$  ( $\Delta$ OCR and  $\Delta Ca^{2+}$ ) were calculated as the difference in steady-state values at 20 mmol/l glucose minus the values at 3 mmol/l glucose. OCR response of  $Ca^{2+}$  channel blockade by nimodipine was represented as the per cent decrement relative to the  $\Delta$ OCR in response to glucose. The per cent decrement in ISR in response to nimodipine was calculated relative to the actual steady-state ISR observed in the presence of 20 mmol/l glucose. Units are pmol/l for insulin, pmol min<sup>-1</sup> (100 islets)<sup>-1</sup> for ISR and nmol min<sup>-1</sup> (100 islets)<sup>-1</sup> for OCR; the ratiometric  $Ca^{2+}$  measurement was unitless. Fasting blood insulin was not measured for the rats used as a source of islets in this study, but was measured for a separate group of rats ranging from 8 to 11 weeks old (fasting plasma insulin concentrations were 187±14 pmol/l (*n*=14) and 189±22 pmol/l (*n*=14), respectively)

\*\*\**p*<0.001 generated from an ANOVA with a post hoc Bonferonni test carried out using Kaleidagraph (Synergy Software). The three values with asterisks were found to be statistically different from both pre- and 1 week-onset values, except for glucose-stimulated ISR whose values from islets that were pre-onset and islets that were harvested 3 weeks after the onset of hyperglycaemia were similar

glc, glucose; nim, nimodipine

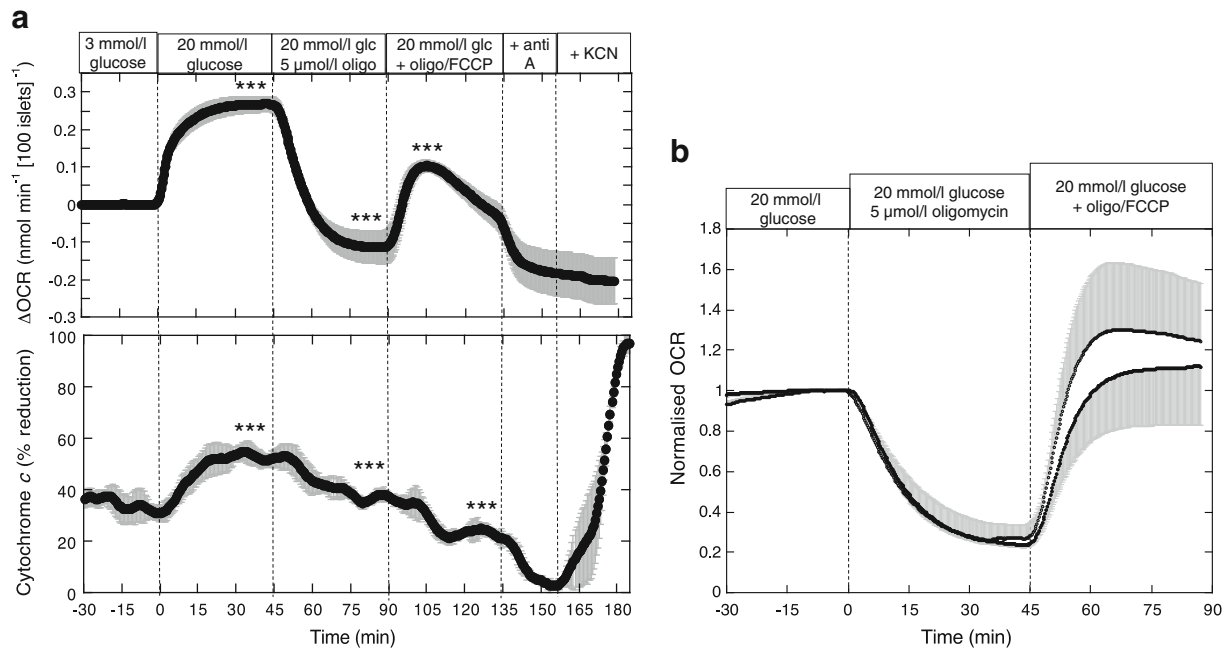


**Fig. 4** Assessment of uncoupling in islets from UCD-T2DM rats. **(a)** Islets were perfused in the presence of 3 mmol/l glucose for 90 min. The glucose in the perfusate was subsequently raised to 20 mmol/l for 45 min, followed by the addition of a blocker of the  $F_0F_1$ ATPase (5  $\mu$ mol/l oligomycin) and subsequent addition of a mitochondrial uncoupler (1  $\mu$ mol/l FCCP). OCR and cytochrome *c* reduction were measured concomitantly using the flow culture system. OCR data is displayed as the change in signal relative to the steady-state value obtained at 3 mmol/l glucose (determined by averaging data obtained in the final 10 min before the increase in glucose). Steady-state OCR at 3 mmol/l glucose was  $0.20 \pm 0.06$  nmol min<sup>-1</sup> (100 islets)<sup>-1</sup> ( $n=6$ ). Cytochrome *c* data were normalised to values obtained in the presence of a blocker of electron flow into cytochrome *c* (antimycin A) and of electron transfer from cytochrome *c* (KCN) as 0% and 100%

respectively, as done previously [18]. The cytochrome *c* data were inherently more inaccurate than OCR, and data smoothing was carried out by calculating moving averages over 6-min intervals. Therefore, the kinetics of the cytochrome *c* data are delayed relative to the OCR data, although the algorithm did not affect the steady-state values that were reached. Data were plotted as mean  $\pm$  SEM. \*\*\* $p < 0.001$ , comparing steady-state values before and after each change in buffer composition (paired *t* test). **(b)** Using the same protocol as in (a), islets harvested from pre-onset (lower curve) and 3 weeks post-onset rats were assessed ( $n=4$ ). To facilitate comparison, data was normalised to the average value attained during the final 5 min of the high-glucose period. To maintain clarity, error bars (representing the SEM) are only shown in a single direction for each curve. No statistical difference between the two curves was detected

**Contribution of mitochondrial uncoupling to  $Ca^{2+}$ -sensitive OCR in UCD-T2DM rat islets** The extent of uncoupling in islets has been assessed by inhibition of the  $F_0F_1$ -ATPase; this stops the dissipation of the proton gradient across the mitochondrial membrane that is supported by electron transport chain activity but not that due to uncoupled proton leak [25, 26]. Accordingly, islets were perfused as in Fig. 2, but instead of blocking  $Ca^{2+}$  channels, the  $F_0F_1$ ATPase was inhibited by oligomycin, followed by the mitochondrial uncoupler carbonyl cyanide-*p*-trifluoromethoxyphenylhydrazone (FCCP). In control islets glucose-stimulated OCR decreased in response to oligomycin by  $82 \pm 1.4\%$  (Fig. 4a) and was increased by the uncoupling agent FCCP, suggesting that mitochondria in normal glucose-stimulated islets are largely coupled. However, simultaneous measurement of cytochrome *c* reduction indicated that some of the OCR decrease may have been due to inhibition of metabolic pathways by the two agents, as cytochrome *c* reduction dropped in parallel with the OCR. Irrespective of the possible error associated with using metabolic poisons, OCR decrements due to oligomycin were similar in

islets from both euglycaemic and 3-week hyperglycaemic UCD-T2DM rats (Fig. 4b) to those observed with control rat islets, indicating that changes in the uncoupling state of

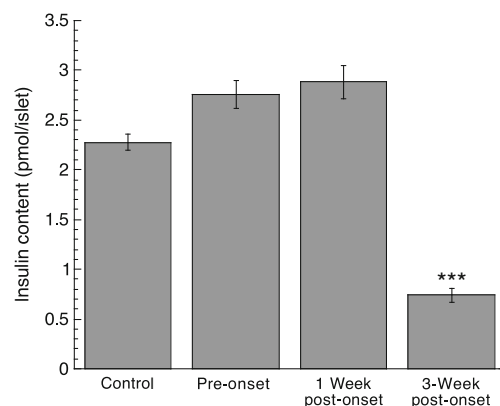


**Fig. 5** Insulin content of isolated islets harvested from control rats and UCD-T2DM rats before, and 1 and 3 weeks after, becoming hyperglycaemic. Data are means  $\pm$  SEM,  $n=3$  or 4. \*\*\* $p < 0.001$  (Student's *t* test)

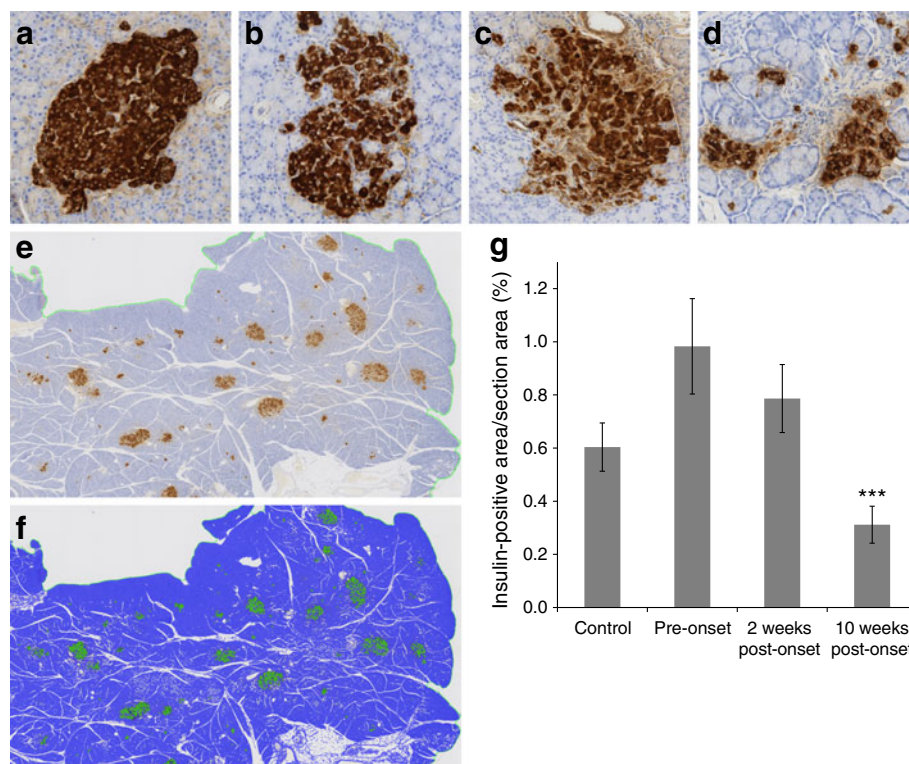


**Fig. 6** Quantification of islet area from pancreas harvested from rats before, and 2 weeks and 10 weeks after, onset of hyperglycaemia. (**a–d**) Representative images from pancreas sections stained for insulin (brown staining) showing islets from Sprague–Dawley controls (**a**) and UCD-T2DM rats before the onset of diabetes (**b**), with recent-onset diabetes (2 weeks after hyperglycaemia) (**c**) or with long-term diabetes (greater than 10 weeks after onset of hyperglycaemia) (**d**). The images show the increased damage to islet morphology as diabetes progressed. (**e, f**). Representative example of output from Visiopharm software

where (**e**) is a stained pancreatic section and (**f**) is the computer-generated identification of insulin-positive (green) or insulin-negative (pancreas; blue) areas. (**g**). Beta cell area expressed as total insulin-positive area / total pancreas area assessed. Number of replicates were 4, 5, 7 and 8, for control, pre-onset, 2 weeks post-onset and 10 weeks post-onset of hyperglycaemia, respectively.  $^{***}p < 0.01$  (ANOVA), where insulin-positive area for islets harvested 10 weeks post-onset was significantly different from insulin-positive area for both 2 weeks post-onset and pre-onset islets

mitochondria are not likely to mediate changes in  $Ca^{2+}$ -sensitive OCR that occurred during this period.

*Insulin content, islet yield and beta cell area during transition to hypoinsulinaemia* Islets from UCD-T2DM rats initially contained insulin stores that were similar to those of the islets from control rats, and then decreased precipitously between 1 and 3 weeks following the onset of hyperglycaemia (Fig. 5). Despite this change in insulin content, secretion was still 70% of that by islets from euglycaemic UCD-T2DM rats (Table 2), suggesting that insulin content had not become limiting. The yield of islets harvested from UCD-T2DM rats was low at all stages compared with the yield from control rats ( $130 \pm 8$  vs  $418 \pm 17$  islets/rat). However, due to the increase in size of islets from UCD-T2DM rats, the total islet volume harvested (calculated by estimating the size of the islet diameter and assuming each islet was spherical) was similar in the two rat strains ( $7.3 \pm 0.5$  vs  $5.9 \pm 0.2 \mu\text{l}$ ).

To determine whether beta cell loss contributed to impaired ISR, the insulin-positive area relative to total

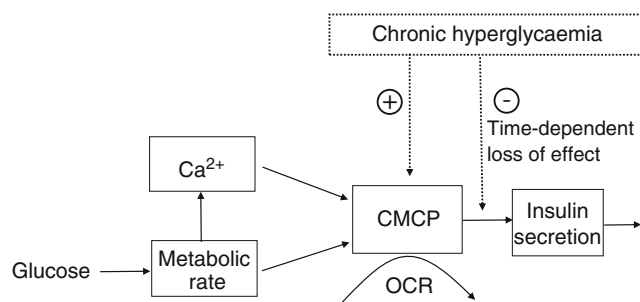


**Fig. 7** Schematic depiction of the normal coupling between  $Ca^{2+}$ , OCR and ISR, and the observed effects seen in the UCD-T2DM rat model. In normal islets, ISR is controlled by  $Ca^{2+}$  influx through L-type  $Ca^{2+}$  channels, and a factor generated when metabolic rate is increased, via a highly energetic process we have termed the CMCP. Sustained ISR only occurs when the CMCP is activated by both  $Ca^{2+}$  and increased metabolic rate. During the transition from hyper- to hypo-insulinaemia occurring between 1 and 3 weeks after onset of hyperglycaemia in the UCD-T2DM rat, islet function is characterised by continually activated CMCP (i.e. not inhibited by  $Ca^{2+}$  channel blockade) and a time-dependent decrease in coupling between CMCP and insulin secretion. We speculate that the continuous operation of the CMCP is energetically unfavourable to islet function and survival

pancreatic area was quantified in pancreas sections. Clear fragmentation and damage to the UCD-T2DM rat islets was evident even before the onset of hyperglycaemia (Fig. 6a–d). However, beta cell area, quantified by an automated imaging system (as illustrated in Fig. 6e, f), tended to be higher in euglycaemic UCD-T2DM rats relative to control rats ( $p=0.12$ ), consistent with the higher OCR at low glucose, and was not decreased in 1-week-onset rats relative to pre-onset UCD-T2DM rats (Fig. 6g). Beta cell area in islets from rats with hyperglycaemia longer than 10 weeks, though, was significantly decreased (Fig. 6g). These data do not support beta cell loss as a primary mediator of the loss of insulin secretory function that occurs early in the course of hyperglycaemia in UCD-T2DM rats.

## Discussion

*Impaired coupling between  $Ca^{2+}$  and OCR was associated with diminished insulin secretory function in vivo* Based on previously obtained data from in vitro experiments showing a tight correlation between the CMCP (as reflected by  $Ca^{2+}$ -sensitive OCR) and ISR [13–15], we hypothesised that loss of CMCP regulation during the progression of the diabetes in the UCD-T2DM model would coincide with the decrease in plasma insulin concentrations during the progression of hyperglycaemia seen in vivo [17]. Glucose-stimulated OCR and  $Ca^{2+}$  did not change significantly in islets harvested following the onset of hyperglycaemia, and glucose stimulation of ISR was still operational in the diabetic islets. Therefore glucose sensing and steps generating an increased energy state leading to closing of  $K_{ATP}$  channels and  $Ca^{2+}$  influx, the standard focus of islet functional analysis, were intact. Our approach to evaluating islet function centred on responses to blocking glucose-stimulated  $Ca^{2+}$  influx, which in normal islets leads to a reproducible decrease in OCR and complete cessation of insulin secretion [14, 15]. The main finding of this study was the demonstration that loss of  $Ca^{2+}$ -sensitivity of OCR and ISR coincided with the decreased plasma insulin levels seen in UCD-T2DM rats. The results are consistent with a link between dysregulation of steps downstream of  $Ca^{2+}$  influx (those comprising the CMCP) and the loss of glucose-stimulated ISR observed after prolonged hyperglycaemia.

*The phenotypic mechanism of insulin release in the UCD-T2DM diabetic islet* A goal of the study was to obtain in vitro data that would generate a candidate mechanism to explain the decline in plasma insulin levels occurring after exposure to chronic hyperglycaemia. Our initial interpretation of the lack of change in OCR of diabetic islets in response to  $Ca^{2+}$  channel blockade was that the CMCP was no longer functional. However, OCR,  $Ca^{2+}$  and ISR were still robustly

stimulated by glucose and, furthermore, insulin secretion was still observable in the presence of  $Ca^{2+}$  channel blockade, indicating that the CMCP was still operational. In islets from control rats, blocking  $Ca^{2+}$  influx by L-type  $Ca^{2+}$  channels abolishes sustained insulin secretion by all known physiological secretagogues including glucose, fatty acids [27] and amino acids [28], as well as potentiators of nutrient-stimulated ISR including acetylcholine and GLP-1 [13]. Thus, the continued secretion of insulin in the presence of nimodipine observed in islets 3 weeks after the onset of hyperglycaemia was unexpected, as was the ability to secrete insulin in response to glucose by islets that do not decrease OCR in response to blocking  $Ca^{2+}$  influx. The most likely explanation for these observations is that the CMCP in diabetic islets remains constitutively activated, which would result in the observed lack of OCR response to nimodipine, thus allowing glucose to stimulate ISR in the presence of nimodipine. This explanation was further supported by results showing that glucose-stimulated OCR was not diminished in these islets. The decrease in insulin levels seen in vivo, in the face of continuously activated CMCP, suggests that the chronically stimulated CMCP does not favour the maintenance of appropriately regulated ISR by the islet (represented schematically in Fig. 7). How this happens is still under investigation, since at this point we have not shown a causal relation between overstimulation of CMCP and decreased ISR. Future work will involve assessing islets from UCD-T2DM rats that are treated with insulin and DPP-4 inhibitors.

*Contribution to the impairment of insulin secretion made by changes in mass vs function* Although it is clear that islets from rats 3 weeks post-onset of hyperglycaemia are functionally impaired, we also considered the potential contributions of loss of insulin content or beta cell area. Although beta cell mass in the UCD-T2DM rat ultimately declines with long-term hyperglycaemia [17], neither islet yield nor beta cell area were decreased during the transition to hypoinsulinaemia (1–3 weeks). Islet insulin content fell dramatically during the transition from hyper- to hypo-secretion of insulin seen in vivo [17]. It seems likely that this was a factor in the impaired secretory function observed in vivo, but the continued robust response of ISR in response to glucose in vitro suggests that content of insulin had not reached levels low enough to become strongly rate limiting. The loss of insulin content could be mediated by the increased energy demands of continuous operation of the CMCP, as suggested by studies where diazoxide, a blocker of the CMCP [15], prevents loss of insulin content in hyperglycaemia [29].

Consistent with increases in beta cell mass typically observed in obese rodents [30, 31], many islets isolated from the UCD-T2DM rats at all stages of glycaemia studied were hyperplastic and over 300  $\mu\text{m}$  in diameter. As would be expected from islets with greater numbers of beta cells,

the overall OCR per islet was much larger (two- to fourfold greater than that observed in normal-sized islets). Since the increased beta cell area was less than twofold that of controls, it follows that the elevated basal OCR might be in part due to greater numbers of non-beta cells. However, the changes in ISR and OCR stimulated by glucose were similar to those seen in the islets from control rats. In addition, since the larger islets harvested from euglycaemic UCD-T2DM rats behaved qualitatively similarly to the control islets, our data does not suggest that hyperplasia of the islets is in itself a factor governing the impairment of function *in vivo* [32]. Neither does increased uncoupling of mitochondria appear to play a role in mediating the transition between normally functioning islets and a lack of  $\text{Ca}^{2+}$ -sensitivity of the OCR. Thus the loss of secretion *in vivo* is most strongly associated with changes in the coupling between  $\text{Ca}^{2+}$ , OCR and ISR, and perhaps changes of insulin biosynthesis, but not with changes in mass or size of the islet population.

*Alternative mechanisms mediating loss of  $\text{Ca}^{2+}$ -sensitive OCR and ISR* Based on the nearly identical cytosolic  $\text{Ca}^{2+}$  responses to glucose, and equal contribution by L-type  $\text{Ca}^{2+}$  channels to this response, by pre- and post-diabetic islets, we favour the conclusion that the loss of  $\text{Ca}^{2+}$ -sensitive OCR and ISR was due to steps downstream of  $\text{Ca}^{2+}$  signalling. However, the method of measurement that we used for determining cytosolic  $\text{Ca}^{2+}$  cannot resolve gradients of  $\text{Ca}^{2+}$  within the cell, particularly in microdomains surrounding the secretory granules. Therefore it cannot be ruled out that even if the overall flux into the cell through L-type  $\text{Ca}^{2+}$  channels was not impaired during the transition to hypoinulinaemia,  $\text{Ca}^{2+}$  may preferentially accumulate in sites away from processes controlling OCR and ISR during the progression of diabetes. In this case, a low CMCP response would be achieved due to lack of stimulation by L-type  $\text{Ca}^{2+}$  channels. In such a scenario,  $\text{Ca}^{2+}$  from other channels could support the continued secretion of insulin in the face of greatly diminished L-type  $\text{Ca}^{2+}$  channel activity.

*Relationship between the phenotype of diabetic islets and subsequent beta cell destruction* Although islet mass remains relatively stable up until 2 months post-onset of hyperglycaemia, previous studies have demonstrated marked disruption of islet structure 3 months after the onset of diabetes [17]. Whether continuous activation of the CMCP is detrimental to islet viability or proliferation was not determined in the present study, although this possibility is supported by studies showing a link between  $\text{Ca}^{2+}$ , endoplasmic reticulum (ER) stress and beta cell death [33, 34]. Consistent with the notion that continued overstimulation of  $\text{Ca}^{2+}$ -activated processes in the beta cell is harmful, it has been shown that diazoxide reduces islet apoptosis and ER stress in the face of exposure to palmitate [35] and

stimulation of  $\text{K}_{\text{ATP}}$  channel activity protects murine pancreatic beta cells against oxidative stress induced by  $\text{H}_2\text{O}_2$  or sulfonylureas [36]. Therefore our findings provide a novel demonstration that constitutive activation of  $\text{Ca}^{2+}$ -stimulated energy usage precedes the destruction of islets in the UCD-T2DM rat and is associated with loss of islet function.

**Acknowledgements** The Visiopharm beta cell quantification analysis algorithm was developed jointly by the Cellular and Molecular Imaging Core of the University of Washington Diabetes Research Center and the Histology and Imaging Core located at the University of Washington.

**Funding** This research was funded by grants from Merck Investigator Initiated Sponsored Program (No. 33171), the National Institutes of Health (DK17047 and DK063986) and the Washington State Life Sciences Discovery Fund. P. J. Havel's laboratory also receives, or received, support during the time the experiments were conducted from NIH grants R01 HL075675, R01 HL091333, AT002599, AT002993, AT003645 and the American Diabetes Association.

**Duality of interest** The authors declare that there is no duality of interest associated with this manuscript.

**Contribution statement** BPC, SCG, RLH, PJH, and IRS made substantial contributions to the conception and design of the study as well as the analysis and interpretation of the data; AMR, BJR, BPC, S-RJ, KLS and JLG contributed a significant quantity of data and method development. All authors participated in the drafting the article or revising it critically for important intellectual content, and gave final approval of the version to be published.

## References

1. Cook DL, Hales CN (1984) Intracellular ATP directly blocks  $\text{K}^+$  channels in pancreatic B-cells. *Nature* 311:271–273
2. Henquin JC (2009) Regulation of insulin secretion: a matter of phase control and amplitude modulation. *Diabetologia* 52:739–751
3. Prentki M (1996) New insights into pancreatic beta-cell metabolic signaling in insulin secretion. *Eur J Endocrinol* 134:272–286
4. Ivarsson R, Quintens R, Dejonghe S et al (2005) Redox control of exocytosis: regulatory role of NADPH, thioredoxin, and glutaredoxin. *Diabetes* 54:2132–2142
5. Corkey BE, Deeney JT, Yaney GC, Tomheim K, Prentki M (2000) The role of long-chain fatty acyl-CoA esters in beta-cell signal transduction. *J Nutr* 130:299S–304S
6. Gembal M, Detimary P, Gilon P, Gao ZY, Henquin JC (1993) Mechanisms by which glucose can control insulin release independently from its action on adenosine triphosphate-sensitive  $\text{K}^+$  channels in mouse B cells. *J Clin Invest* 91:871–880
7. Jung SR, Kuok IT, Couron D et al (2011) Reduced cytochrome *c* is an essential regulator of sustained insulin secretion by pancreatic islets. *J Biol Chem* 286:17422–17434
8. Kibbey RG, Pongratz RL, Romanelli AJ, Wollheim CB, Cline GW, Shulman GI (2007) Mitochondrial GTP regulates glucose-stimulated insulin secretion. *Cell Metab* 5:253–264

9. Pi J, Bai Y, Zhang Q et al (2007) Reactive oxygen species as a signal in glucose-stimulated insulin secretion. *Diabetes* 56:1783–1791
10. Jensen MV, Joseph JW, Ilkayeva O et al (2006) Compensatory responses to pyruvate carboxylase suppression in islet beta-cells. Preservation of glucose-stimulated insulin secretion. *J Biol Chem* 281:22342–22351
11. MacDonald MJ, Fahien LA, Brown LJ, Hasan NM, Buss JD, Kendrick MA (2005) Perspective: emerging evidence for signaling roles of mitochondrial anaplerotic products in insulin secretion. *Am J Physiol Endocrinol Metab* 288:E1–E15
12. Hasan NM, Longacre MJ, Stoker SW et al (2008) Impaired anaplerosis and insulin secretion in insulinoma cells caused by small interfering RNA-mediated suppression of pyruvate carboxylase. *J Biol Chem* 283:28048–28059
13. Jung SR, Reed BJ, Sweet IR (2009) A highly energetic process couples calcium influx through L-type calcium channels to insulin secretion in pancreatic beta-cells. *Am J Physiol Endocrinol Metab* 297:E717–E727
14. Gilbert M, Jung SR, Reed BJ, Sweet IR (2008) Islet oxygen consumption and insulin secretion tightly coupled to calcium derived from L-type calcium channels but not from the endoplasmic reticulum. *J Biol Chem* 283:24334–24342
15. Sweet IR, Gilbert M (2006) Contribution of calcium influx in mediating glucose-stimulated oxygen consumption in pancreatic islets. *Diabetes* 55:3509–3519
16. Ortsater H, Liss P, Akerman KE, Bergsten P (2002) Contribution of glycolytic and mitochondrial pathways in glucose-induced changes in islet respiration and insulin secretion. *Pflugers Arch* 444:506–512
17. Cummings BP, Digitale EK, Stanhope KL et al (2008) Development and characterization of a novel rat model of type 2 diabetes mellitus: the UC Davis type 2 diabetes mellitus UCD-T2DM rat. *Am J Physiol Regul Integr Comp Physiol* 295:R1782–R1793
18. Sweet IR, Cook DL, DeJulio E et al (2004) Regulation of ATP/ADP in pancreatic islets. *Diabetes* 53:401–409
19. Matsumoto S, Shibata S, Kirchoff N (1999) Immediate reversal of diabetes in primates following intraportal transplantation of porcine islets purified on a new histidine-lactate-iodixanol gradient. *Transplantation* 67:S220
20. Sweet IR, Cook DL, Wiseman RW et al (2002) Dynamic perfusion to maintain and assess isolated pancreatic islets. *Diabetes Technol Ther* 4:67–76
21. Sweet IR, Khalil G, Wallen AR et al (2002) Continuous measurement of oxygen consumption by pancreatic islets. *Diabetes Technol Ther* 4:661–672
22. Jung SR, Reed BJ, Sweet IR (2009) A highly energetic process couples calcium influx through L-type calcium channels to insulin secretion in pancreatic beta-cells. *Am J Physiol Endocrinol Metab* 297:E717–E727
23. Nobes CD, Brown GC, Olive PN, Brand MD (1990) Non-ohmic proton conductance of the mitochondrial inner membrane in hepatocytes. *J Biol Chem* 265:12903–12909
24. Abe Y, Sakairi T, Kajiyama H, Shrivastav S, Beeson C, Kopp JB (2010) Bioenergetic characterization of mouse podocytes. *Am J Physiol Cell Physiol* 299:C464–C476
25. Wikstrom JD, Sereda SB, Stiles L et al (2012) A novel high-throughput assay for islet respiration reveals uncoupling of rodent and human islets. *PLoS One* 7:e33023
26. Affourtit C, Brand MD (2006) Stronger control of ATP/ADP by proton leak in pancreatic beta-cells than skeletal muscle mitochondria. *Biochem J* 393:151–159
27. Warnotte C, Gilon P, Nenquin M, Henquin JC (1994) Mechanisms of the stimulation of insulin release by saturated fatty acids. A study of palmitate effects in mouse beta-cells. *Diabetes* 43:703–711
28. Sener A, Somers G, Devis G, Malaisse WJ (1981) The stimulus-secretion coupling of amino acid-induced insulin release. Biosynthetic and secretory responses of rat pancreatic islet to L-leucine and L-glutamine. *Diabetologia* 21:135–142
29. Yoshikawa H, Ma Z, Bjorklund A, Grill V (2004) Short-term intermittent exposure to diazoxide improves functional performance of beta-cells in a high-glucose environment. *Am J Physiol Endocrinol Metab* 287:E1202–E1208
30. Steil GM, Trivedi N, Jonas JC et al (2001) Adaptation of beta-cell mass to substrate oversupply: enhanced function with normal gene expression. *Am J Physiol Endocrinol Metab* 280:E788–E796
31. Liu YQ, Jetton TL, Leahy JL (2002) Beta-cell adaptation to insulin resistance. Increased pyruvate carboxylase and malate-pyruvate shuttle activity in islets of nondiabetic Zucker fatty rats. *J Biol Chem* 277:39163–39168
32. Hayek A, Woodside W (1979) Correlation between morphology and function in isolated islets of the Zucker rat. *Diabetes* 28:565–569
33. Huang CJ, Gurlo T, Haataja L et al (2010) Calcium-activated calpain-2 is a mediator of beta-cell dysfunction and apoptosis in type 2 diabetes. *J Biol Chem* 285:339–348
34. Duchon MR (2004) Roles of mitochondria in health and disease. *Diabetes* 53(Suppl 1):S96–S102
35. Sargsyan E, Ortsater H, Thorn K, Bergsten P (2008) Diazoxide-induced beta-cell rest reduces endoplasmic reticulum stress in lipotoxic beta-cells. *J Endocrinol* 199:41–50
36. Gier B, Krippeit-Drews P, Sheiko T et al (2009) Suppression of KATP channel activity protects murine pancreatic beta cells against oxidative stress. *J Clin Invest* 119:3246–3256